Combustion characterization of hybrid methane-hydrogen gas in domestic swirl stoves.

LIU, X., ZHU, G., ASIM, T. and MISHRA, R.

2022

Combustion Characterization of Hybrid Methane-Hydrogen Gas in Domestic Swirl Stoves

Xiaozhou Liu [a], Guangyu Zhu [a], Taimoor Asim [b*], Rakesh Mishra [c]

[a] Guangdong University of Technology, China

[b] School of Engineering, Robert Gordon University, UK (AB10 7GJ)

[c] School of Computing & Engineering, University of Huddersfield, UK (HD1 3DH)

Corresponding Author: +44(0)1224 262457; t.asim@rgu.ac.uk

Abstract: Combustion of hybrid natural gas (methane) and hydrogen mixture in domestic swirl stoves has been characterized using hot-state experiments and numerical analysis. The detailed combustion mechanism of methane and hydrogen (GRI-Mech 3.0) has been simplified to obtain reduced number of chemical reactions involved (82 % reduction). The novel simplified combustion mechanism developed has been used to obtain combustion characteristics of hybrid methane-hydrogen mixture. The difference between the calculations from the detailed and the simplified mechanisms has been found to be < 1 %. A numerical model, based on the simplified combustion model, is developed, rigorously tested and validated against hot-state tests. The results depict that the maximum difference in combustion zone's average temperature is < 13 %. The investigations have then been extended to hybrid methane-hydrogen mixtures with varying volume fraction of hydrogen. The results show that for a mixture containing 15 % hydrogen, the release of CO due to combustion reduces by 25 %, while the combustion zone's average temperature reduces by 6.7 %. The numerical results and hot-state tests both confirm that the temperature remains stable when hybrid methane-hydrogen mixture is used in domestic swirl gas stoves, demonstrating its effectiveness in cooking processes.

Keywords: Swirl Gas Stoves, Hybrid Methane-Hydrogen Mixture, Hot-State Tests, Numerical Simulations, CO emission.

1.0 Introduction

The Paris Agreement emphasis on the development of low-carbon and zero-carbon solutions to achieve carbon neutrality [1]. As it is a legally binding international treaty, countries all over the world are concentrating their efforts to reduce dependence on carbon-based fuels, which can have significant impact on reducing environmental pollution. The exponential increase in the use of coal in China from 2000 to 2010 has become stable since 2015 as it looks to gradually replace coal with natural gas as the primary source of energy [2]. The second most energy consuming sector in China is domestic (after industrial) where natural gas is becoming increasingly popular for heating and cooking purposes. For cooking, the majority households use swirl gas stoves, with CO being the main pollutant emitted [3]. If China has to fulfil its commitment to make non-fossil fuel energy only 20 % of its total energy supply, it will have to look towards carbon-zero fuels, such as Hydrogen, to be adopted as the primary fuel for domestic applications. At present, adding hydrogen to natural gas is an effective means to reduce hazardous CO emissions and improve the thermal efficiency of gas stoves. An important question arises here that how much hydrogen can be added to methane in domestic stoves.

Haeseldonckx et al. [4], through calculating the Warburg number, concluded that when < 17 % of hydrogen is mixed in the natural gas pipeline (in Belgium), the hybrid gas can be safely used in domestic and commercial stoves. Hu et al. [5] designed a constant volume combustion

chamber system and analysed it through the use of schlieren high-speed photography. Experimental results show that when the hydrogen concentration is < 60 %, the combustion state is dominated by methane combustion. A transitional state has been observed for hydrogen concentration between 60 % and 80 %. When hydrogen concentration is > 80 %, methane inhibits combustion of hydrogen. Donohoe et al. [6] conducted experiments to measure ignition delay time in shock tubes and fast compressors. Chemkin software was used to simulate the experimental data, while the results were consistent with the experiments. Experimental results show that the ignition delay time decreases with the increase of temperature, pressure, hydrogen mixing ratio and the increase of long-chain hydrocarbons. Ahmed et al. [7] conducted experiments and numerical simulations to explore the effects of hydrogen doping on the chemical structure of methane flames under sooting conditions. The results show that the addition of hydrogen affects the chemical microstructure of methane flame while keeping the C/O ratio and the cold gas flow rate constant. Ying et al. [8] studied the detailed chemical effects of hydrogen as a fuel additive on the laminar premixed methane / air flame. The dilution and thermal effects lead to the addition of hydrogen in the flame, which reduces the molar fraction of C_2H_2 and CH_2CO, and also reduce the formation of oxygen-containing pollutants CH_2O and CH_3CHO.

As the combustion characteristics of hydrogen are substantially different from those of natural gas (methane), extensive investigations need to be carried out in order to better understand the complex combustion characteristics of a mixture of methane and hydrogen. With a perspective of potential use of hybrid methane-hydrogen mixture in domestic gas stoves, Luo et al. [9] studied the combustion safety and emission performance of the fuel composed of

hydrogen and natural gas on domestic gas appliances. The experimental results show that the flame stability and flue gas emissions meet the requirements of national standards. Zhao et al. [10] studied the combustion characteristics of fuel gas under different hydrogen doping concentrations. The results show that although doping hydrogen effectively reduce the emission of pollutants, when the volume of hydrogen doping in fuel gas is 20 %, backfire will occur in domestic gas stoves. Jiang et al. [11] used numerical simulations to study the effects of primary air coefficient, fire hole cone angle and pot support height on the thermal efficiency of domestic gas stoves. Although the optimal influence factor combination under orthogonal experimental conditions was obtained, but it was not experimentally verified. Chen et al. [12] studied the influence of different primary air coefficient on the flame shape of high-power domestic gas stove under the same power through numerical simulation. Pashchenko [13] conducted a detailed study of hydrogen-rich combustion in a swirling flame using Computational Fluid Dynamics (CFD) and found that an increase in the hydrogen mole fraction leads to an increase in the combustion temperature. Hydrogen-rich fuel blends produce less nitrogen oxides than pure methane. Sun et al. [14] studied the effect of mixing hydrogen in natural gas at a volume ratio of 0-20 % on the performance of domestic gas appliances. The results show that when the volume of mixed hydrogen is 25 %, backfire will occur in the domestic gas water heater. Jones et al. [15] analyzed the feasibility of mixing hydrogen based on the natural gas characteristics and terminal equipment in the UK. When the hydrogen content increases, the parameter area where backfire may occur is expanded. By adjusting the shape and angle of the burner, the swirl flame can be formed to improve the flame stability. Zhao et al. [16] evaluated the interchangeability of hydrogen and natural gas for residential

commercial oven burners and concluded that addition of hydrogen will reduce the ignition time. It has been reported that the ignition backfire limit is a state with 25 % hydrogen concentration. Compared with pure natural gas, adding 10 % hydrogen increases the burner temperature by 63 %. Moreover, addition of hydrogen does not significantly change NO_X emission level, but reduces the CO emission.

As hydrogen is combustible and explosive, at present, researchers around the world generally use numerical methods to investigate the combustion performance of hydrogen doped natural gas. The detailed mechanism used in this study is the GRI-MECH 3.0 [17] combustion model, which is widely used in the study of methane and hydrogen combustion characteristics. The GRI-Mech 3.0 reaction mechanism contains 53 component and 325 reactions, however, the computational power required to carry out these calculations is prohibitive, often requiring the use of supercomputer facilities. If a simplified version of the detailed combustion model is developed, it will significantly aid in reducing the computational requirements, but the accuracy of the simplified model will need to be verified against the detailed model. Sensitivity Analysis (SA) is often used in the simplification of combustion mechanism and has been widely used in recent years. Hou et al. [18] developed a 10-step 12-component simplified combustion mechanism suitable for methane rocket engine through sensitivity analysis. This mechanism is consistent with the detailed mechanism for the prediction of equilibrium temperature and main concentration. Jiang et al. [19] simplified the 58-step elementary reaction through sensitivity analysis for the combustion characteristics of piston engine. The simplified model can accurately predict the premixed combustion phenomenon in the engine. Wang et al. [20] simplified the model of 15-components for Perfectly Stirred Reactor (PSR) model by

110 combining temperature sensitivity and production rate, which is suitable for the combustion of
111 phenolic resin pyrolysis products in air under supersonic conditions, in which the pyrolysis gas
112 includes H_2O, CH_4, CO, H_2, CO_2 etc. Ruan et al. [21] developed the full mixed-flow reaction
113 model through the PSR model. Through the reaction path, it was found that the main NCO free
114 radicals and N_2O free radicals in the NO compound reduction reaction were significantly
115 affected by the temperature. Increasing the temperature was conducive to the generation and
116 consumption of NCO and N_2O free radicals, which is beneficial to the reaction.

117 The Direct Relation Graph (DRG) method [22] has also been widely used in combustion
118 mechanism simplification. Fany et al. [23] simplified the detailed mechanism of Dodecane
119 combustion by using DRG and Calculation Singular Value Perturbation method. The
120 calculation results show that the simplified mechanism can reproduce the simulation results of
121 Dodecane in the aspects of ignition delay time, flameout and species concentration distribution
122 under high temperature combustion condition. Lu et al. [24] and Poon et al. [25] carried out
123 further research work and simplified the combustion mechanism by using the two-step DRG
124 method and observed that the calculation efficiency of this mechanism significantly improved.
125 Monnier et al. [26] simplified the RAMEC mechanism through the direct relationship graph
126 with error propagation (DEGEP) [27] and verified the simplified mechanism through the one-
127 dimensional premixed flame model. Results show that temperature difference between the
128 simplified mechanism and the detailed mechanism is 4 %, and the calculation speed is
129 increased by 8 times compared to the detailed mechanism. Simplified mechanism can
130 accurately calculate the combustion results of methane and oxygen under high pressure
131 conditions. Tang et al. [28] simplified the mechanism after the coupling of kee-58 mechanism

and Aramco Mech 1.3 according to the directed relationship graph method (DRGEPSA) [29] combining sensitivity analysis and error analysis for the combustion of methane and dimethyl ether at the micro scale. Results of simulation calculation based on simplified mechanism are the same as the flame shape and flameout limit in the experiment. Hu et al. [30] simplified the USC mech II mechanism under the high-pressure oxygen enriched combustion condition through the directed relationship graph method and time scale reduction analysis. Difference between the high-pressure oxygen enriched combustion flame calculated by the simplified mechanism and the detailed mechanism is within 10 %. Li et al. [31] simplified the detailed mechanism based on AramcoMech 2.0 mechanism through the directed relationship graph method for the mixed combustion of ammonia, hydrogen and methane. Simplified mechanism has been simulated in the coaxial common flow burner with turbulent non-premixed jet flame. Results are in close agreement with the detailed mechanism, and the calculation time is only 20 % of the detailed mechanism.

Based on the GRI-Mech 3.0 mechanism, the simplified methane-hydrogen combustion mechanism with 26 components and 143 reactions was obtained by Gimeno-Escobedo et al [17] using Chemkin software. It is verified by the calculation results in a zero-dimensional homogeneous reactor and one-dimensional free flame propagation, which shows that the error is kept within a reasonable range. The simplified mechanism reduces the number of chemical reactions by 56 % compared to the conventional detailed mechanism. In the present study, a simplified combustion mechanism for hybrid methane-hydrogen mixture to be used in domestic gas stoves has been developed using Sensitivity Analysis (SA) and Direct Relationship Graph (DRG) methods. The novel mechanism reduces the number of chemical

reactions of the detailed mechanism by 82 %, thus decreasing the computational power required significantly. The simplified mechanism is then implemented in the numerical solver for the combustion analysis. The numerical predictions have been validated against experimental results through hot-state tests. The effectiveness of the simplified combustion model is compared with the detailed model through comparative analysis, providing a reference basis for the wide application of hybrid methane-hydrogen gas in domestic swirl gas stoves.

2.0 Development of the Simplified Combustion Mechanism

The simplified combustion mechanism model developed in the present study is based on the Perfectly Stirred Reactor (PSR) model in CHEMKIN, which is a software widely used for solving complex chemical kinetics in a wide variety of combustion applications [32]. PSR [33] is a Fortran program that predicts the steady-state temperature and species composition in a PSR. The reactor in this model is characterized by a reactor volume, residence time or mass flow rate, heat loss, reaction temperature and the mixture composition. The model accounts for finite-rate elementary chemical reactions. The governing equations are a system of nonlinear algebraic equations. The program solves these equations using a hybrid Newton/time-integration method. The program runs in conjunction with the CHEMKIN package, which handles the chemical reaction mechanism. The PSR model has been used to study combustion mechanism of fuel in this study as the combustion condition described by this model is similar to that of a gas stove. The available chemical reaction kinetic model for combustion modelling of methane and hydrogen with oxygen has been simplified using Sensitivity Analysis (SA), Direct Relation Graph (DRG) and DRG with Error Propagation (DRGEP) techniques. The simplified chemical reaction kinetic model obtained has then been analyzed in detail.

2.1 Temperature Sensitivity Analysis

The detailed chemical reaction mechanism (GRI-Mech 3.0) is simplified using sensitivity analysis method, and the temperature sensitivity analysis of overall and key components has been carried out for the full reaction process of methane and hydrogen mixture in air. The overall sensitivity analysis result is shown in figure 1. It can be seen from that the combustion reaction is mainly promoted by H+O_2<=>O+OH (R13). This reaction converts O_2 into the concentration of O radical and accelerates combustion. The reactions of negative temperature sensitivity coefficient are mainly H+CH_4<=> CH_3+H_2 (R24) and OH+CH4<=>CH_3+H_2O (R30). In the actual combustion process, R24 and R30 consume H radical and OH radical, which slows down the oxidation rate. It should be noted that the time when the sensitivity coefficient of each elementary reaction reaches the peak is different, and the peak point of each reaction is selected in the subsequent analysis.

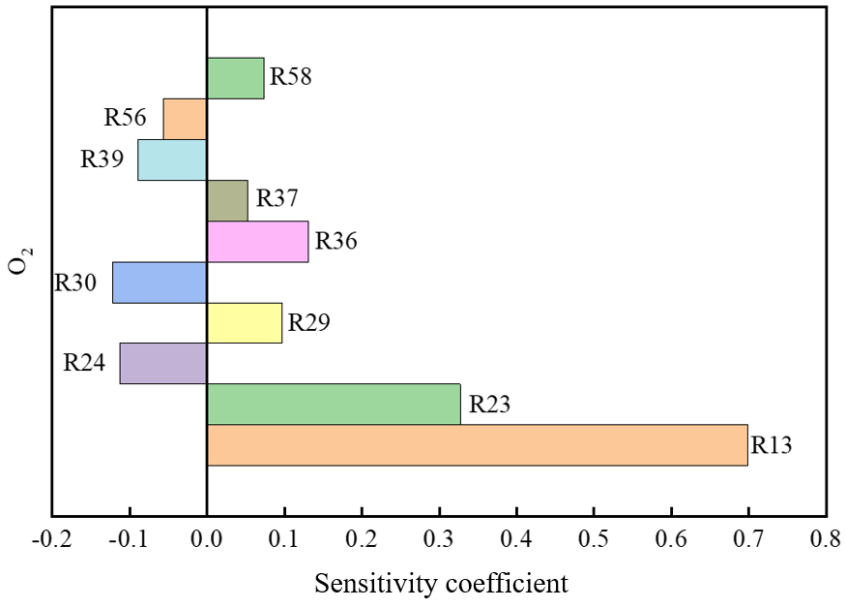

Figure 1. Overall temperature sensitivity analysis

The equations included in the overall temperature sensitivity are summarized in table 1. It is evident that H_2, O_2, CH_4, CH_3 and OH are the key reaction components. The sensitivity analysis has been carried out to analyze the temperature sensitivity of all the key components. Further simplification of the whole reaction process is achieved by removing the elementary reaction with small sensitivity coefficient and retaining the elementary reaction with large sensitivity coefficient.

Table 1. Key reaction equations

R13	$H+O_2<=>O+OH$
R23	$H+CH_3(+M)<=>CH_4(+M)$
R24	$H+CH_4<=>CH_3+H_2$
R29	$OH+CH_3<=>CH_2(S)+H_2O$
R30	$OH+CH_4<=>CH_3+H_2O$
R36	$CH_2+CH_4<=>2CH_3$
R37	$CH_2(S)+N2<=>CH_2+N_2$
R39	$CH_2(S)+O_2<=>CO+H_2O$
R56	$O+CH_3=>H+H_2+CO$
R58	$CH_2+O_2=>2H+CO_2$

The sensitivity analysis results of the key components are shown in figure 2. It can be seen that there is a certain difference between the temperature sensitivity of the base component and the temperature sensitivity of the total reaction. However, the reactions with higher absolute value of temperature sensitivity are the same for the reactions R13, R24, R23, R30 and R36.

These reactions contain important elementary units, which are H, O, O_2, OH, CH_3, CH_4, H_2 and H_2O.

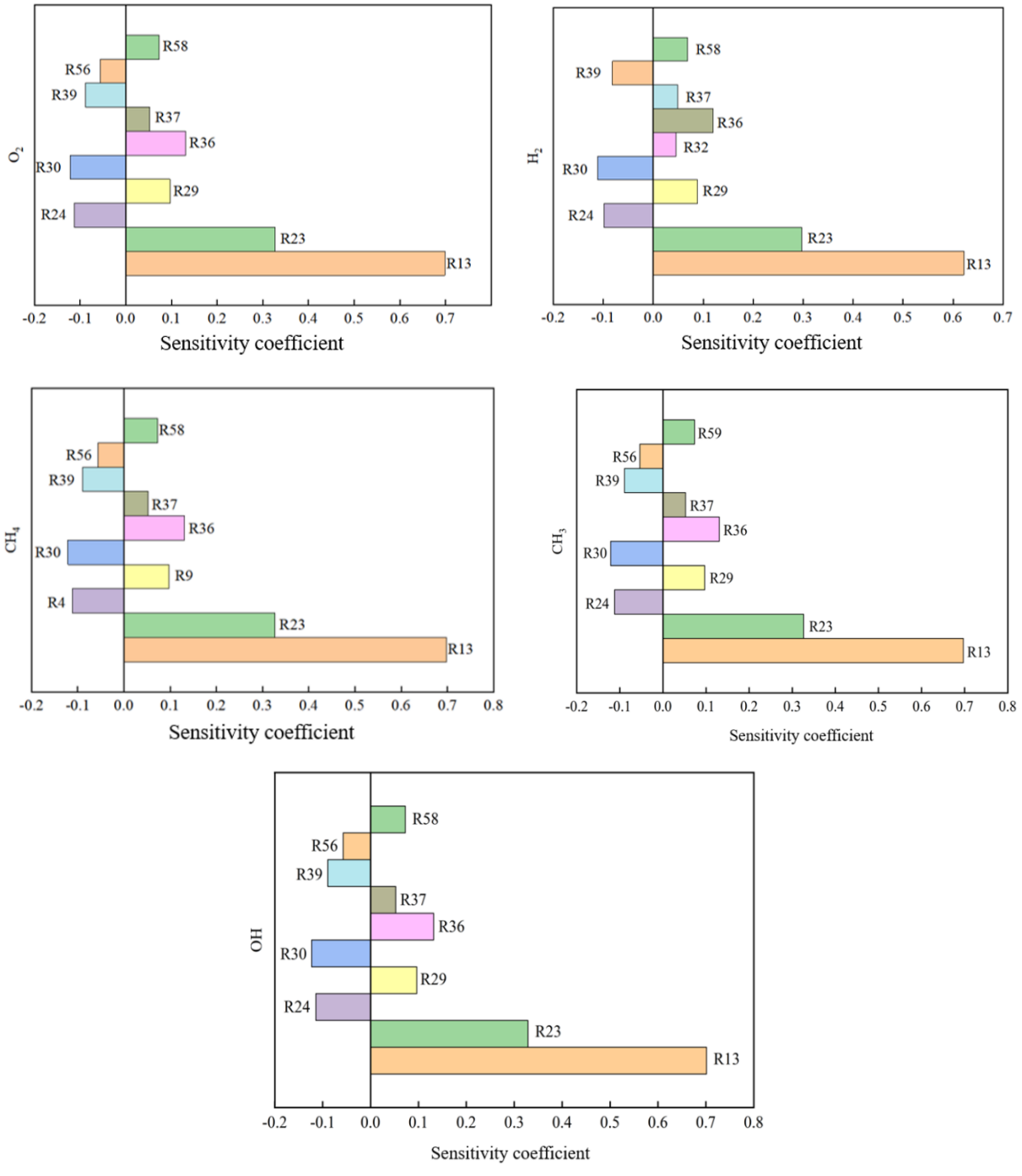

Figure 2. Sensitivity analysis of O_2, H_2, CH_4, CH_3 and OH

2.2 Direct Relation Graph

The elementary units identified through sensitivity analysis are further simplified using Direct Relation Graph (DRG) method [22]. This method can effectively simplify the secondary components and elementary reactions in the detailed mechanism, but also have some shortcomings. DRG ignores the weakening of the correlation between components when propagating along the path. In order to reduce the error caused by the simplification of one-step DRG, this study adopts the method of DRG combined with Error Propagation (EP), thus resulting in DRGEP method [27]. In the simplification process, the key elementary components (H, O, O_2, OH, CH_3, CH_4, H_2 and H_2O) and reaction products (CO and CO_2) obtained from the sensitivity analysis are searched as the initial component set, and the obtained component set is coupled with the important components of the initial detailed mechanism. The calculated results of different sample points are then combined to obtain the final reaction component set. The reaction equation with the components contained in the set is regarded as an important reaction, and its equation is retained to construct a simplified mechanism.

In order to achieve this, the combustion conditions of the hybrid methane-hydrogen gas mixture are simplified and PSR model is implemented. The calculation condition of this PSR model is set as follows: the initial reaction temperature is T = 1800 K, the pressure is P = 1 atm and the residence time is t = 0.01 s. The values of these parameters are derived from the data of the gas stove in normal operation. Because methane has a very high calorific value, its maximum combustion temperature reaches as high as 1800 K. Furthermore, since the reaction speed of methane is extremely fast, the reaction time is taken as 0.01s in this paper. P is defined as 1 atm, which means that the combustion experiment is carried out under atmospheric

conditions. The volume of the reactor is 282 cm^3. Ignoring the heat loss, the mole fractions of CH_4, H_2 and O_2 are 0.109, 0.05 and 0.183 respectively, and the equivalence ratio is 1.6. The absolute error and relative error in the simplification process are set to 10^{-5} and 10 % respectively. The mechanism simplified by DRG method is 72 steps reaction of 19 components. DRGEP method is used to continue the simplification. The original 53 component and 325 steps reaction model is simplified to 17 component and 58 steps reactions model, which significantly reduces the calculation workload. The complete simplified reaction model is provided in the appendix.

In order to verify the accuracy of the simplified model developed, the results calculated using this model are compared against the results obtained from the detailed model. The comparative analysis depict that the simplified mechanism is applicable to the calculation of pure methane and methane-hydrogen doping conditions, as shown in figure 3. It can be seen that by deleting some components, the generated substances in some reactions reduce after simplification, and the chain activation reaction lags behind, resulting in the change of position of the flame. With the passage of time, when the combustion is in a stable state, the error between the two mechanisms is no more than 1 %, which proves the validity of the simplified mechanism.

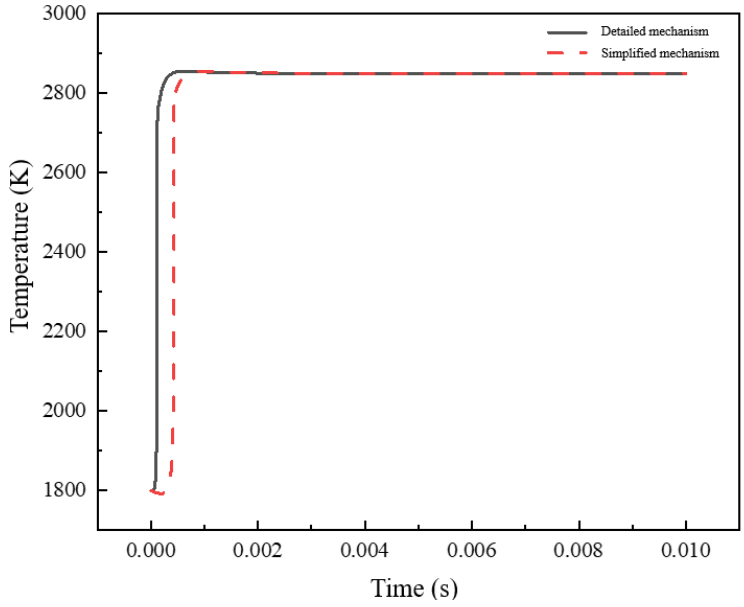

(a)

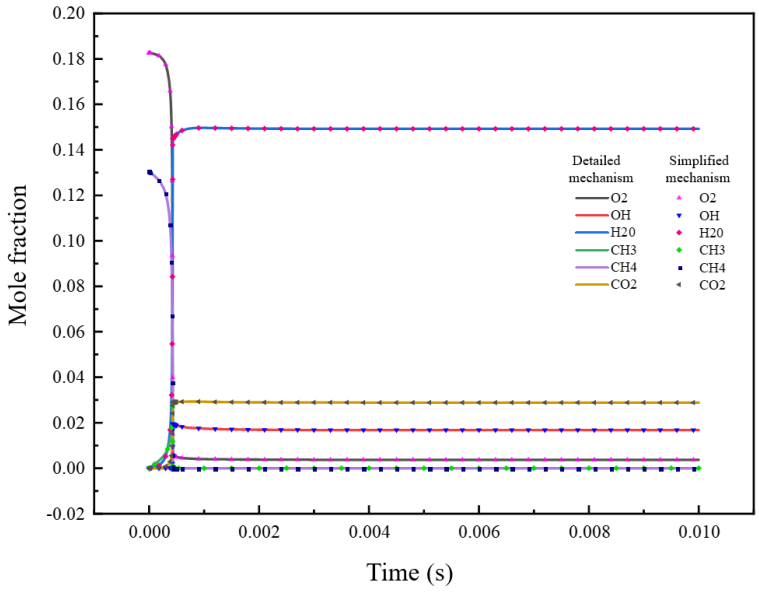

(b)

Figure 3. Comparison of (a) temperature and (b) mole fraction of the key components from the simplified and the detailed mechanisms

3.0 Numerical Combustion Analysis of Methane in a Swirl Gas Stove

The simplified mechanism developed in this study is applicable to the combustion of both pure methane and hybrid methane-hydrogen mixture. This section provides details of

combustion of methane only, while the combustion characteristics of hybrid methane-hydrogen mixture are presented in section 4. The experimental validation of the numerical results has been carried out for the combustion of methane and hybrid methane-hydrogen mixture (with 15 % Hydrogen).

3.1 Geometric Model of the Swirl Gas Stove

A typical domestic swirl gas stove is shown in figure 4. It consists of two burner rings and a heat-resistant quartz plate on top. These gas stoves are widely used in China in the domestic sector for cooking purposes. Luo et al. [34] have reported that swirling enhances the supplement and mixing function of secondary air and is conducive to more complete combustion, thus making swirl gas stoves more efficient than straight gas stoves.

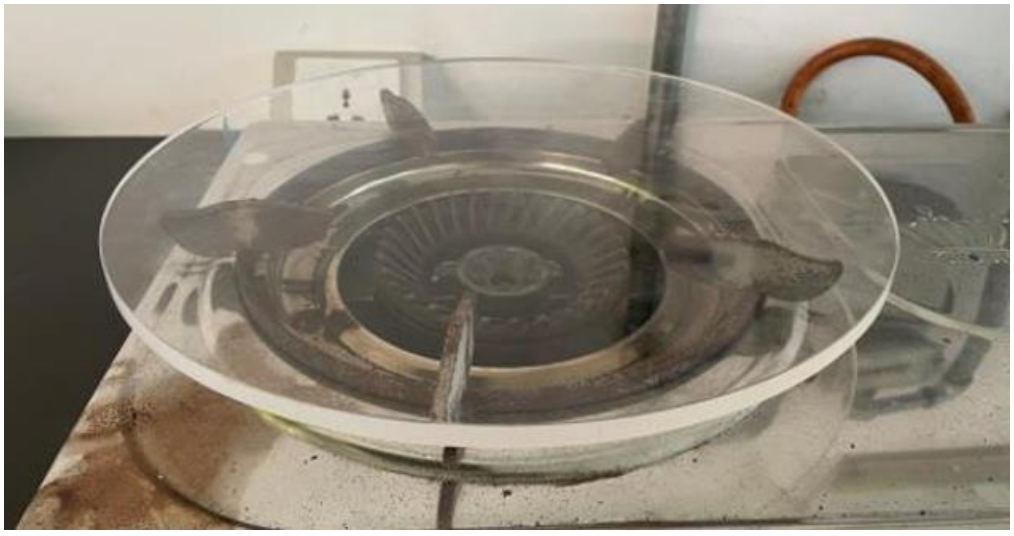

Figure 4. Swirl gas stove

Based on the swirl gas stove shown in figure 4, a geometric model has been created in ANSYS® [35], as shown in figure 5. The stove comprises of two parts i.e. the burner and the quartz plate on top of the burner. The burner has two rings i.e. the outer ring and the inner ring;

271 each ring has its own inlet. The dimensions of the different geometric features of the model are
272 summarized in table 2.

273 Table 2. Geometric details of the swirl gas stove model

Feature	Dimension
Outer Ring diameter	120 mm
Outer Ring Inlet	13.5 mm
Inner Ring dimeter	10.3 mm
Inner Ring Inlet	11.9 mm x 0.1 mm
Inner Ring Fire Holes diameter	1.95 mm
Burner Height	37 mm
Burner's Horizontal Inclination	14 °
Burner's Vertical Inclination	11.7 °
Quartz Plate's diameter	320 mm
Quartz Plate's thickness	8 mm

274

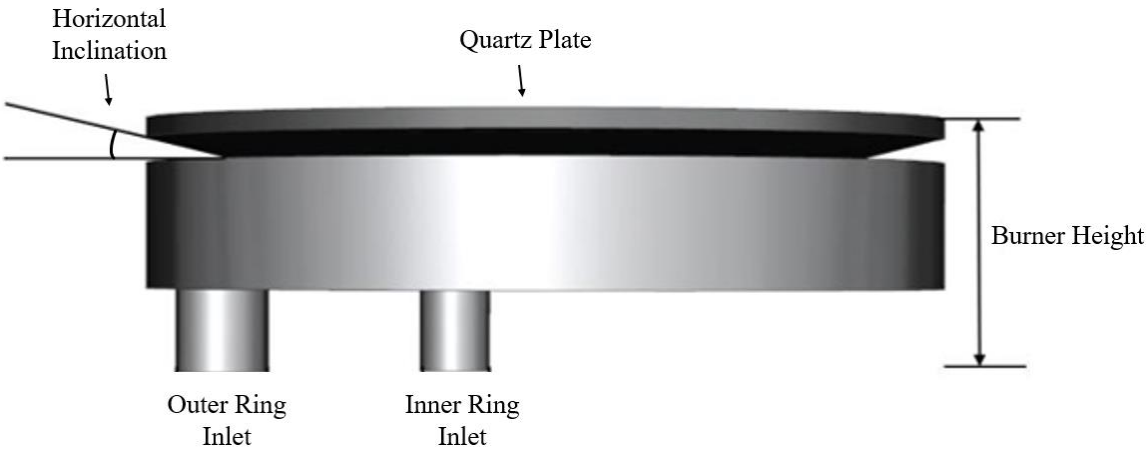

275

276 (a)

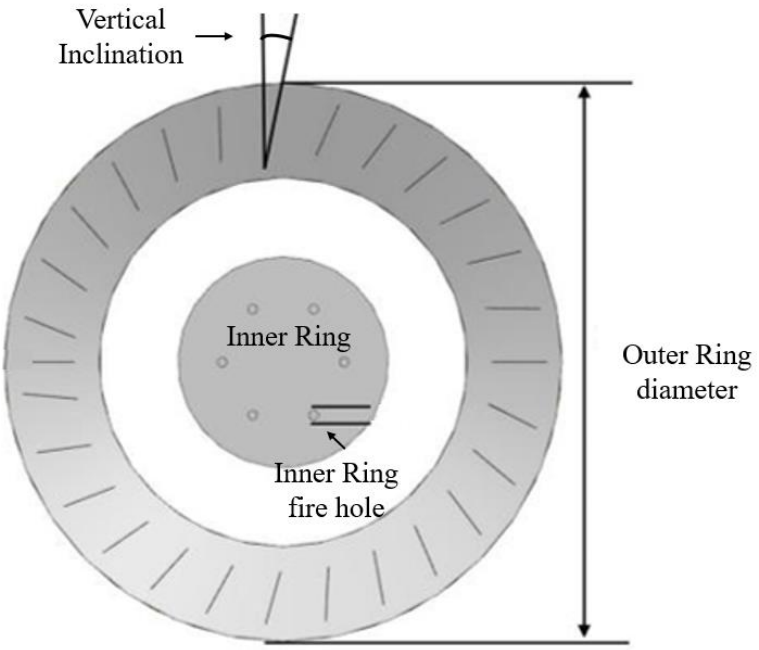

277

278 (b)

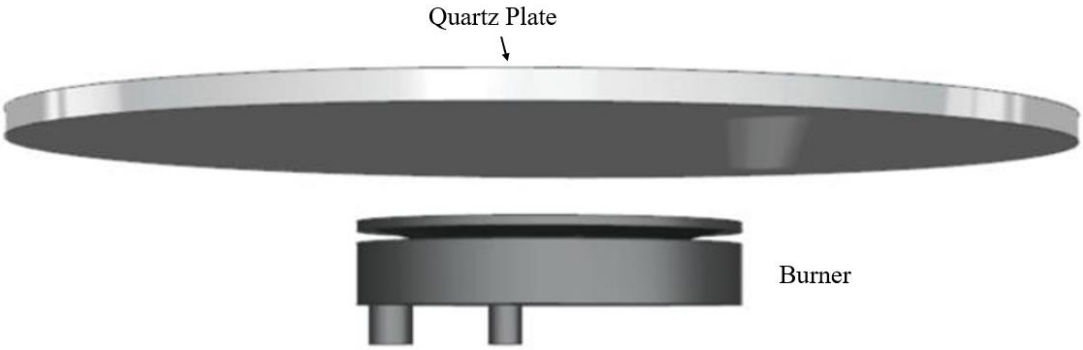

279

280 (c)

281 Figure 5. Geometric model of the swirl gas stove a) burner; b) rings of the burner; c)

282 complete model

283 Since the fuel is evenly distributed after entering the premixing chamber, the model is

284 axially symmetrical and thus, $1/6^{th}$ of the model has been used for further modelling, as shown

285 in figure 6.

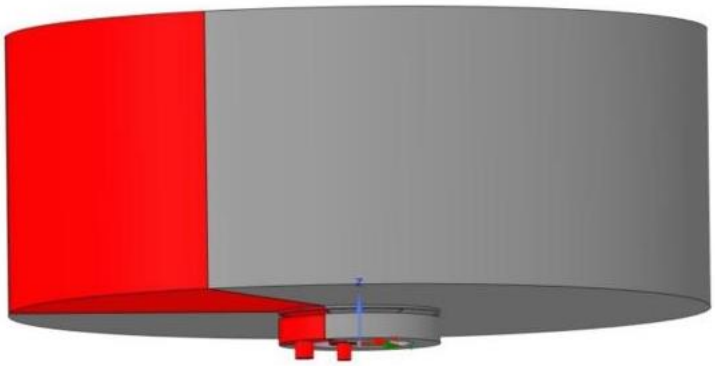

Figure 6. 1/6th model of the swirl gas stove (highlighted)

3.2 Spatial Discretization of Swirl Gas Stove's Flow Domain

The flow domain of the swirl gas stove is a cylinder with a diameter of 500 mm and a height of 200 mm. An unstructured mesh comprising of polyhedral elements has been generated in the flow domain [36]. The density of the mesh elements in the combustion zone i.e. in the vicinity of the fire holes is kept relatively higher compared to rest of are the flow domain. The meshed flow domain is shown in figure 7(a). In order to ascertain the independence of numerical predictions from the density of mesh elements in the flow domain, a number of meshes have been generated. The parameter that has been chosen for mesh independence tests is the flow velocity at the exit of fire holes. It can be seen in figure 7(b) that as the number of mesh elements increases from ~ 1 x 10^5 to ~ 2 x 10^5, the flow velocity at the exit of fire holes decreases from 2.84 m/s to 2.70 m/s (4.9 % decrease). On further increasing the mesh density to ~ 3 x 10^5, the flow velocity remains almost the same. Thus, the mesh with ~ 2 x 10^5 elements has been chosen for numerical analysis in the present study.

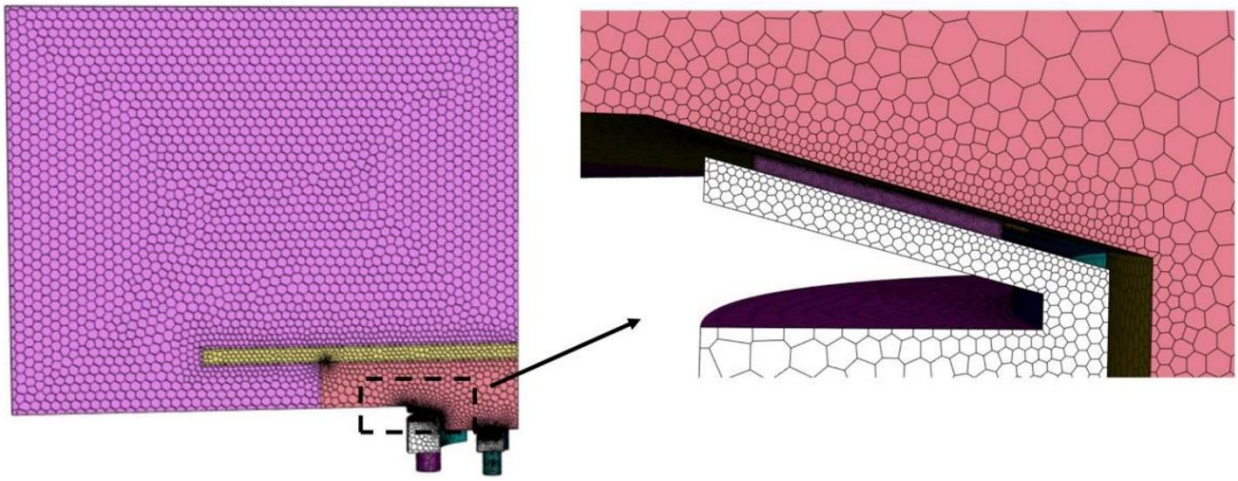

(a)

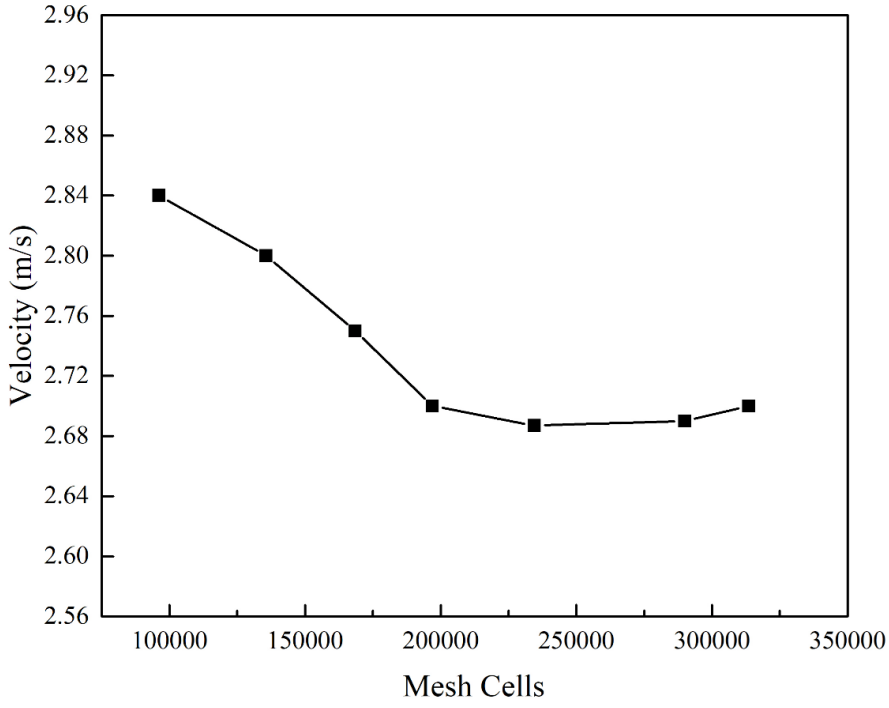

(b)

Figure 7. (a) Meshing of the swirl gas stove's flow domain (b) Mesh independence test results

3.3 Specifications of the Boundary Conditions

The boundary types specified to the swirl gas stove model are shown in figure 8. It can be seen that top surface of the model (A) is the outlet of the combustion products and has been

modelled as a pressure outlet. The circumferential surface (B) is the secondary air inlet and has been modelled as a pressure inlet boundary. Surfaces C_1 and C_2 are the inlets of inner and outer rings respectively and thus, have been modelled as velocity inlets. Surface D is the heat-resistant quartz plate which has been modelled as a solid wall with thermal coupling between the solid and fluid regimes. Surface F is the periodic boundary (due to symmetry) and surface E has been specified as the adiabatic wall. Since the upper half of the heat-resistant quartz plate is the flue gas outlet, the mesh density is higher in this region (see figure 7).

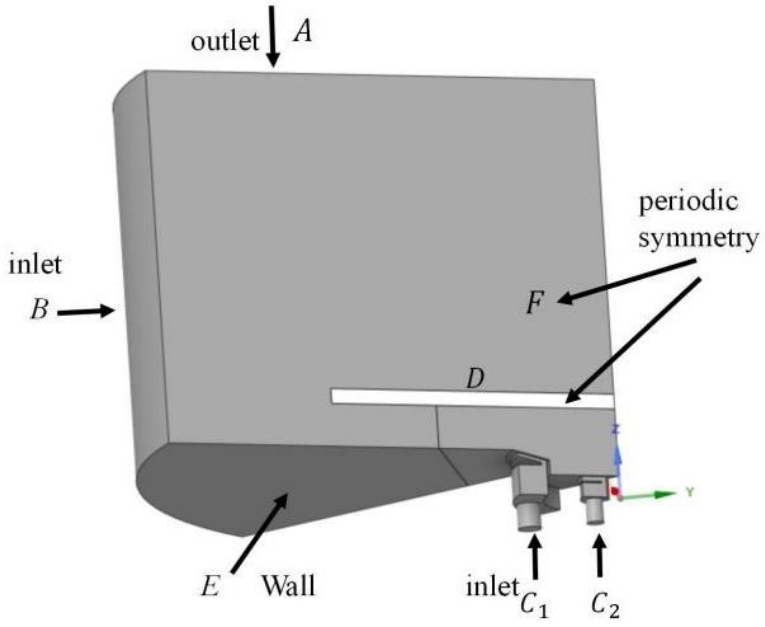

Figure 8. Boundary conditions for the swirl gas stove model

The boundary conditions specified to the numerical model of the swirl gas stove have been summarized in table 3. The calculated load of the gas stove is 3.8 kW and the equivalence ratio is ~ 1.6.

Table 3. Boundary conditions

Boundary	Velocity (m/s)	Hydraulic diameter (cm)	Mole fraction	Temperature (K)
Inner ring inlet	0.15	0.92	CH_4:0.159, O_2:0.18	315
Outer ring inlet	0.25	1.25	CH_4:0.159, O_2:0.18	315
Air inlet	-	80	O_2:0.2181	300
Air outlet	-	50.8	-	-

3.4 Combustion Modelling

The Finite Rate Model (FRM) has been employed in the present study as the combustion model. In order to avoid errors caused by frequency factor and activation energy in the reaction rate, a double precision solver is used in the calculation process. The governing equation of combustion reaction is:

$$R_i = M_{w,i} \sum_{r=1}^{N_R} R_{i,r} \quad (1)$$

where $M_{w,i}$ is the molar molecular weight of component I and $R_{i,r}$ is the Arrhenius molar rate of generation/decomposition of component i. When the reaction proceeds in the forward direction, the governing equation of the forward reaction constant $k_{f,r}$ is:

$$k_{f,r} = A_r T^{\beta_r} e^{-E_r/RT} \quad (2)$$

where A_r is the frequency factor, β_r is temperature index (dimensionless), E_r is the activation energy in the reaction (J/kmol) and R is the general gas constant. When the reaction proceeds in reverse direction, the governing equation of the reverse reaction constant is:

$$k_{b,r} = \frac{k_{f,r}}{K_r} \quad (3)$$

where K_r is the equilibrium constant of reaction r. The chemical reaction mechanism (GRI-Mech 3.0), which is applicable to both pure methane and hydrogen doped methane, has been simplified above, and this model has been used for numerical investigations and experimental validation in this study.

3D Navier-Stokes equations have been iteratively solved for steady flow of combustion gases in the flow domain. Turbulence in the flow has been modelled using 2-equation Shear Stress Transport k-ω model [37]. The simplified combustion mechanism is incorporated into the component transport model. The SIMPLE algorithm is used to couple the flow velocity and pressure, while the momentum and energy equations have been discretized using second-order upwind method.

3.5 Temperature Distribution on the Quartz Plate

Thermal variations on the top surface of the heat-resistant quartz plate have been obtained through numerical simulations, which have then been validated against the experimental data obtained. The aim here is to ascertain the appropriateness of the numerical modelling approach used, which can then be extended to carry out the numerical combustion modelling of hybrid methane-hydrogen mixture in the same swirl gas stove. The thermal variations shown in figure 9 indicate that the temperature in middle region of the quartz plate is significantly higher

compared to the temperature along the periphery of the quartz plate. Thus, thermal gradient in the radial direction of the quartz plate is visible. Looking closely at figure 5 (c), it is evident that the high temperature on the quartz plate is due to the burner rings directly under this region.

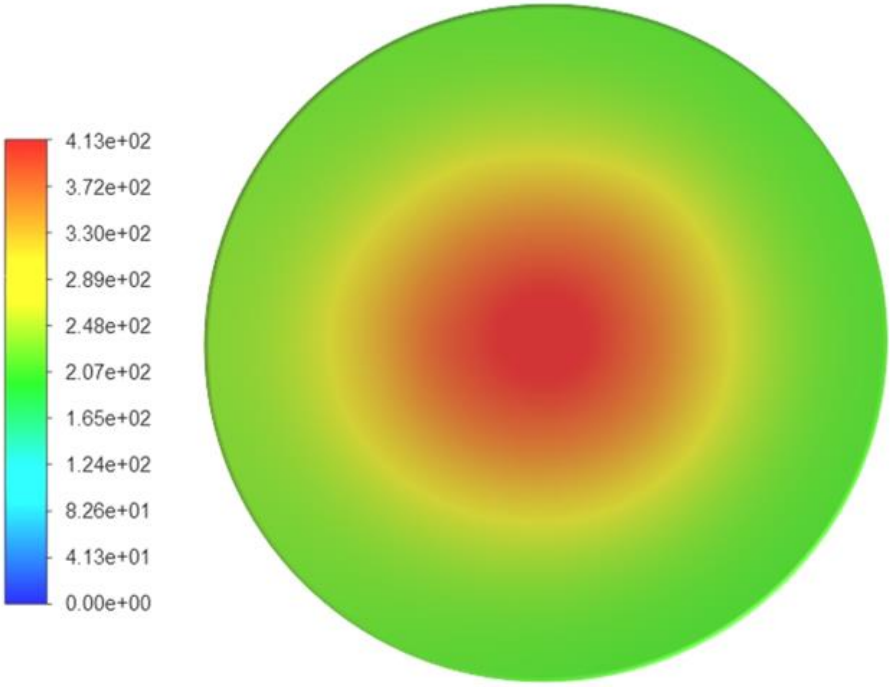

Figure 9. Static temperature (in °C) variations on the heat-resistant quartz plate

3.6 Experimental Validation of Methane Combustion

The thermal and velocity fields associated with domestic swirl gas stoves are very difficult to measure directly as the temperature is quite high. Therefore, in the present study, the method adopted by Vijaykumar Hindasageri [38] has been used for thermal characterization of the swirl gas stove. During the experiments, thermal image of the heat-resistant quartz plate has been obtained after stable combustion has been achieved. Thermal stability is gauged through the stability in the temperature readings, with variations not exceeding 5 ℃. The thermal image has been captured using an infrared imager FLUKE TiX640, which has a measurement range of -40 ℃ to 1200 ℃, and a measurement error of not more than ± 1.5 ℃.

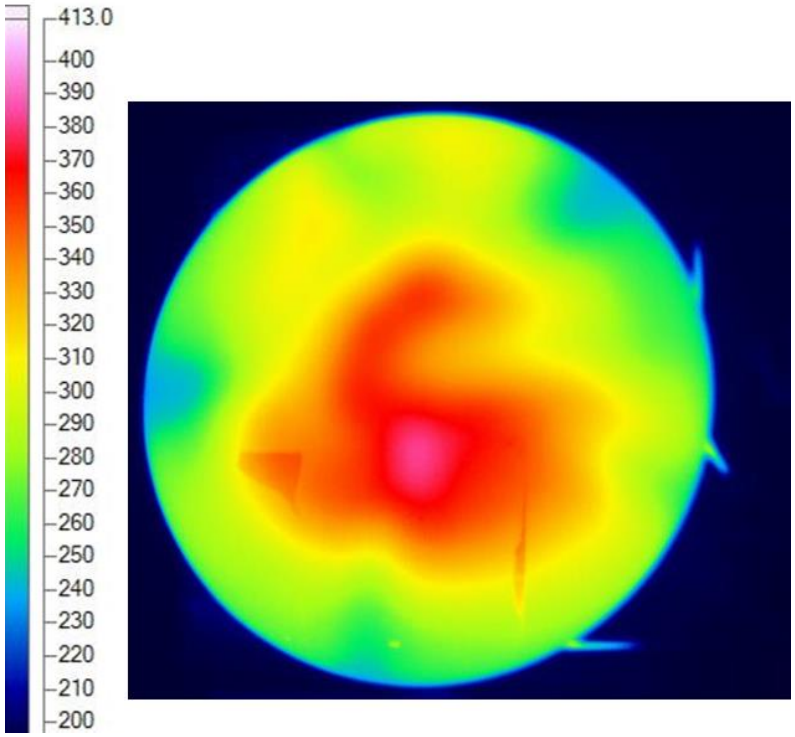

Figure 10. Thermal image of the heat-resistant quartz plate (°C)

Figure 10 depicts the temperature variations on the top surface of the heat-resistant quartz plate. As observed in case of numerical thermal analysis of the plate, it can be seen that the temperature is considerably higher in the middle region of the plate, while the temperature is lower in the peripheral regions. Moreover, it is observed that the temperature profile measured experimentally on the quartz plate is quite non-uniform in comparison with the numerically predicted temperature profile. The primary contributor to this difference is the geometrical differences between the two environments; the experiments are performed in an open space while the numerical modelling is carried out in a small cylindrical domain. Experimental investigations carried out by Zheng [39] indicate that the heat loss from the flue gas accounts for ~ 18 % of the total heat loss. It can be seen in figure 10 that at the edge of the quartz plate, the flue gas begins to surge upward, resulting in significant amount of heat loss, which makes the temperature field uneven. There is a need to carry out extensive quantitative analysis to

highlight the differences between the two methodologies employed in this study. It should however be noted that the scaling used in figures 9 and 10 are different; the maximum scale value is the same but the minimum scale value is different.

As mentioned earlier, a detailed quantitative analysis is required in order to evaluate the differences between the experimental and the numerical results. This has been carried out in this study using the equal section method proposed by Jin et al. [40]. Average temperature values are computed on a series of circular paths on the top surface of the heat-resistant quartz plate, as shown in figure 11. The radii of these paths are 75 mm, 100 mm, 125 mm and 150 mm respectively.

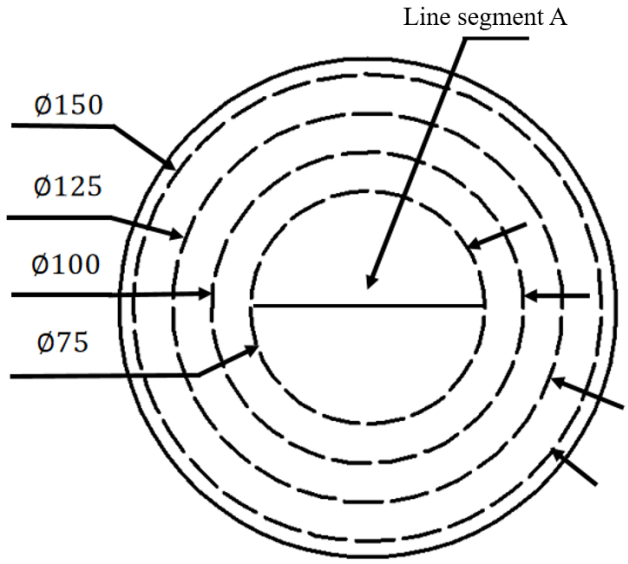

Figure 11. Local paths for thermal comparison

The average temperature values on these circular paths have been summarized in table 4. It can be seen that as the radius of the circular paths increase (radially outwards on the quartz plate), the difference between the numerically predicted and experimentally recorded average temperature values increases. It can be seen from that the average temperature predicted by the

numerical solver at the periphery of the heat-resistant quartz plate (150 mm) is ~ 13 % lower than recorded experimentally. There are two potential reasons for this difference in temperature. The first reason is the geometrical variations in the manufacturing of the gas stove. While the gas stove has been numerically modelled as a perfectly symmetrical body with accurate geometric dimensions, the same is not possible during its manufacturing due to the deviations caused during the machining processes. The diameter of outer rings fuel outlets of the gas stove is slightly bigger than the numerical model. This causes slightly higher gaseous fuel ejection from the outer rings in hot-state tests. Therefore, the experimentally measured temperature is higher than the numerically predicted temperature, especially when the radius increases. This leads to non-uniformities in the thermal characteristics of the gas stove, as evident in figure 10. The second reason for this difference is that in the numerical solver, the heat transfer from the quartz plate to the ambient air takes place in the horizontal direction only, whereas during the experiment, the heat transfer to the ambient air can take place in any direction. Therefore, the heat transfer in the vertical direction is prominent, resulting in the experimental temperature values being higher than numerically predicted temperature.

These temperature differences between the experimental and numerical models are within an acceptable range (< 15 %) [41-43] and thus, the accuracy of the numerical solver employed in this study is verified.

Table 4. Average temperature values on the circular paths

Radius (mm)	Temperature (°C)		Difference w.r.t. experimental values (%)
	Numerical	Experimental	
75	346.7	346.8	0.03
100	303.6	317.7	4.44
125	260.8	292.2	10.75
150	242.3	272.2	12.98

Further analyzing the temperature differences between the experimental and numerical investigations, focusing on the region directly above the burner/rings of the swirl gas stove, temperature values have been recorded on the line segment A shown in figure 11. The length of this line is 150 mm and it passes through the center of the quartz plate. It can be seen in figure 12(a) that the maximum temperature recorded experimentally is ~ 380 °C, while the maximum temperature recorded numerically is ~ 427 °C. Thus, the difference in the maximum temperature values is ~ 47 °C (or ~ 12 %), which is consistent with the maximum temperature difference summarized in table 4. Moreover, figure 12(b) depicts the deviation in experimentally and numerically recorded temperature.

Based on these results, it can be concluded that the numerical methodology adopted in this study is capable of predicting thermal variations associated with the combustion of gases in a swirl gas stove with reasonable accuracy, and thus, it can be used for conducting thermal analysis for the combustion of hybrid methane-hydrogen mixture.

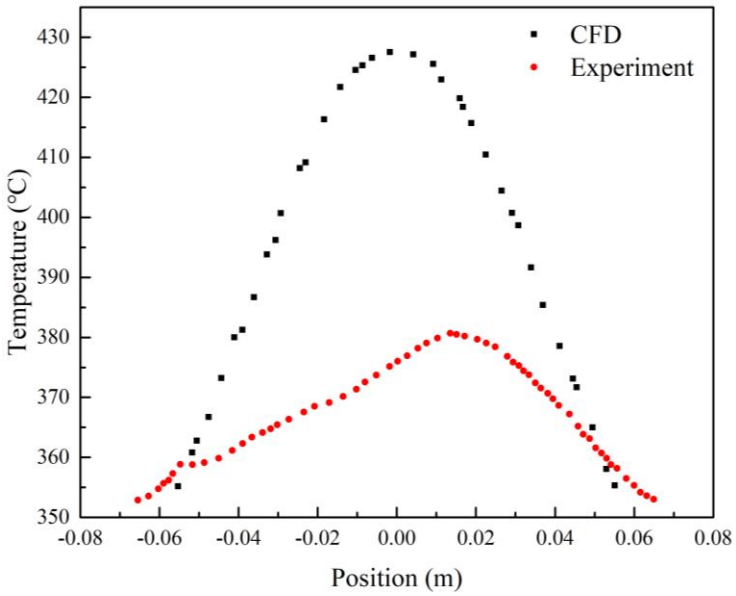

(a)

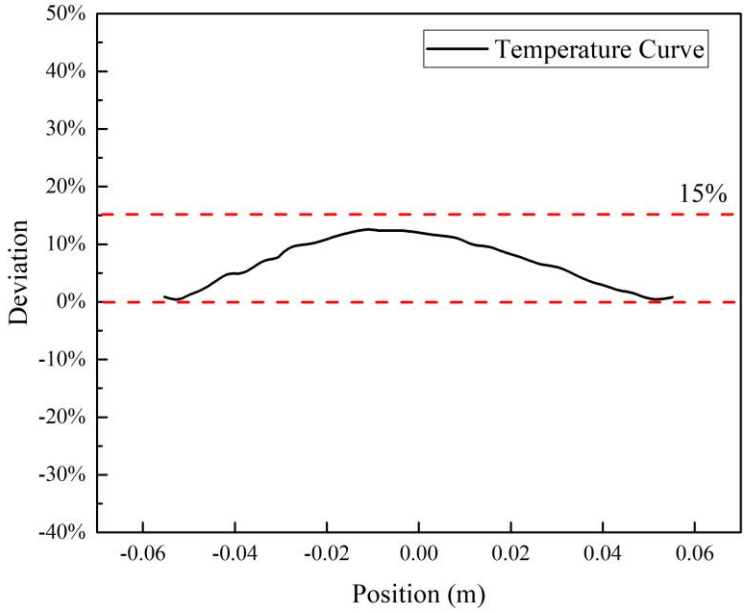

(b)

Figure 12. (a) Local temperature variations on line segment A (b) Deviation between experimental and numerical local temperature measurements

4.0 Numerical Combustion Analysis of Hybrid Methane-Hydrogen Mixture in a Swirl Gas Stove

It is a well-known fact that hydrogen is a highly flammable and explosive gas having

NFPA 704's highest rating of 4 (NFPA: National Fire Protection Association). Thus, great attention should be paid towards safety when considering hydrogen for combustion purposes. Wu [44] has stated that the explosion limit of hydrogen concentration in air is 4 % by volume i.e. < 4 % hydrogen can be mixed in air for ignition and complete combustion. Similarly, the required volumetric ratio of methane in air for complete combustion is 1:10 i.e. the concentration of methane in combustion supporting air is 10 %. When hybrid methane-hydrogen is to be used for combustion purposes, the mixing ratio of hydrogen can be upto 40 %. Combining the aforementioned statistics, it can be concluded that when hybrid methane-hydrogen mixture is to be used with combustion supporting air, the volumetric concentration of hydrogen cannot be > 4 %.

Based on the calculation of interchangeability between methane and hydrogen, under the condition of meeting the high Wobbe number and combustion potential of natural gas, the maximum volumetric concentration of hydrogen in natural gas cannot be > 23 %. Zhao et al. [10] have found through experimental investigations that backfire and deflagration will occur when hydrogen, with a volume fraction of 20 %, is added to the natural gas. Considering the safety aspects of hydrogen combustion, the numerical modelling carried out in the present study does not exceed hydrogen concentration of 15 %; the numerical investigations have been carried out on hybrid methane-hydrogen mixture, where the volume fraction of hydrogen is 5 %, 10 % and 15 % respectively. The numerical results of these investigations are discussed in the sections below.

4.1 Thermal Analysis

Wind gate controlling has been adopted to ensure that the excess air coefficient remains unchanged under different hydrogen concentrations. Figure 13 depicts the variations in total temperature within the flow domain for different concentrations of hydrogen (0 % to 15 %). It can be seen that as the concentration of hydrogen increases, the maximum temperature of the flame gradually decreases.

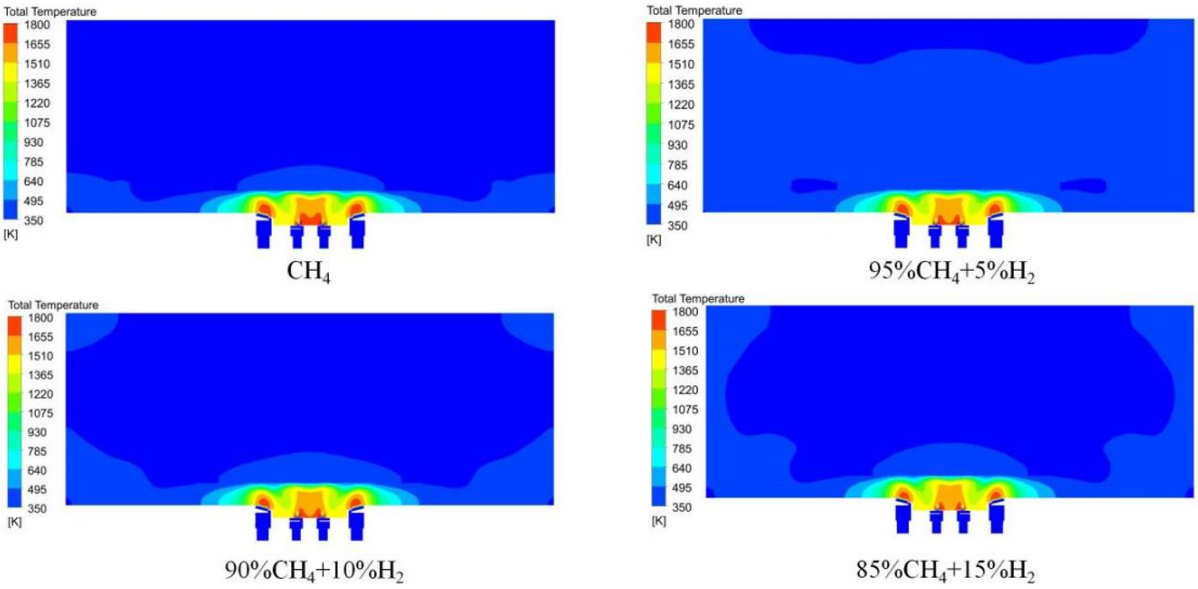

Figure 13. Total temperature variations for different volumetric concentrations of hydrogen

In order to carry out quantitative thermal analysis, thermal profiles are down at the outlet of fire holes shown in figure 13. Figure 14 depicts that the temperature at the exit of fire holes (x = -0.05 m, 0 m and 0.05 m) is high, as expected, while the temperature in the gap regions between the fire holes is relatively lower. Moreover, the temperature away from the fire holes is significantly lower. This is true for all the different concentrations of hydrogen considered in the present study. It can also be seen that as the volumetric concentration of hydrogen in methane increases, the maximum temperature at the exit of the fire holes decreases. Table 5

summarizes the maximum temperature data taken from figure 14. It can be seen that when 5 % hydrogen is added to methane, the maximum temperature at the exit of the fire holes decreases by 1.5 %. Further increasing hydrogen's volumetric concentration to 10 % decreases the maximum temperature by further 1.5 %, and when hydrogen's concentration reaches 15 %, there is a further ~ 1.5 % decrease in maximum temperature. Thus, it can be concluded that every 5 % increase in the volumetric concentration of hydrogen decreases the maximum temperature by 1.5.

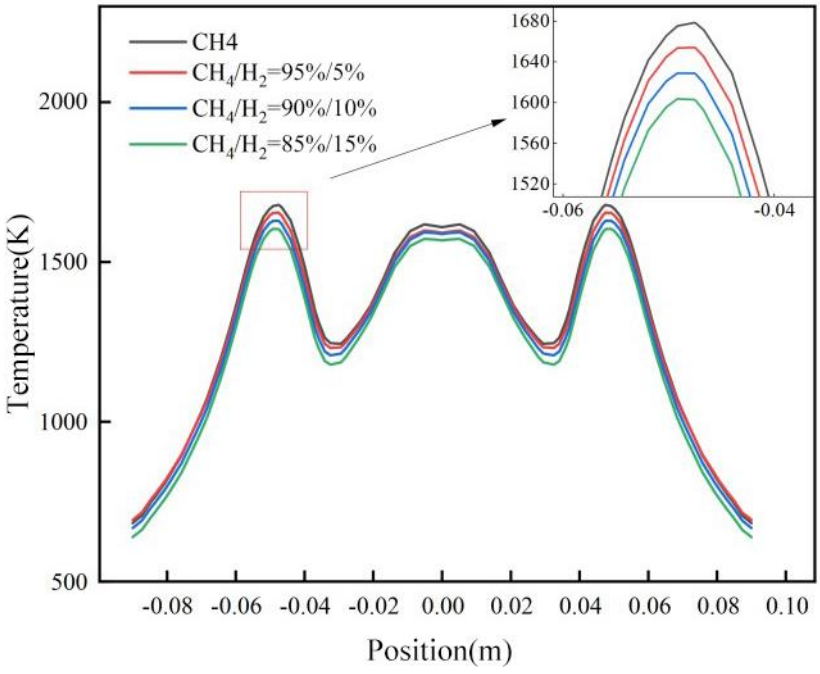

Figure 14. Temperature distribution at the exit of fire holes for different concentrations of hydrogen

The question arises that why the combustion temperature decreases when methane is doped with hydrogen. The low calorific values of methane and hydrogen are ~ 35.81 MJ/m^3 and ~ 10.78 MJ/m^3 respectively. Thus, the combustion of low calorific value hydrogen gas results in lowering the overall temperature of combustion. More the concentration of hydrogen

492 in methane, lower the calorific value of the mixture, because hydrogen is added to the mixture
493 in volume proportion. The molecular weight, density and mass of hydrogen is less than that of
494 methane. The overall density and calorific value of the mixed fuel are less than those of pure
495 methane. The volume average temperature in the flow domain for 0 %, 5 %, 10 % and 15 %
496 hydrogen concentrations have been computed to be 886 K, 875 K, 857 K and 827 K
497 respectively. In comparison with the volume average temperature of pure methane, the
498 temperature in the flow domain decreases by 1.2 % (5 % H_2), 3.3 % (10 % H_2) and 6.7 % (15 %
499 H_2) respectively. It is noteworthy here that although the percentage decrease in maximum
500 temperature at the fire holes' outlets has been observed to be constant with increasing hydrogen
501 concentration, the percentage decrease in average temperature in the flow domain increases.

502 Table 5. Maximum temperature variations

Hydrogen Concentration (%)	Maximum Temperature (K)	Difference w.r.t. 0 % concentration (%)
0	1680	-
5	1655	1.5
10	1629	3.0
15	1603	4.6

503 **4.2 Combustion Products Analysis**

504 When a carbonaceous fuel is burned incompletely, CO is produced, which has serious
505 health risks for humans as it is highly toxic gas which is colorless and odorless. The production

506 of CO is considerably affected by the combustion temperature; lower combustion temperature
507 leads to more production of CO [45]. It has been observed in the previous section that hybrid
508 methane-hydrogen mixture results in lower combustion temperature. This has the potential to
509 produce more CO. However, at the same time, hydrogen is not a carbonaceous gas, thus the
510 combustion of hydrogen cannot lead to any carbon gases. There is a need to carry out a detailed
511 analysis on the combustion products from hybrid methane-hydrogen mixture in order to find
512 out whether this mixture results in more or lower CO production.

513 Figure 15 depicts the variations in CO mole fraction for different hydrogen concentrations
514 under consideration (i.e. 0 %, 5 %, 10 % and 15 %). It can be clearly seen that the CO
515 production from pure methane combustion is high, as expected, and thus, higher CO mole
516 fraction distribution is evident under the heat-resistant quartz plate, from where CO then
517 disperses radially outwards into the ambient air. As the volumetric concentration of hydrogen
518 increases, significant decrease in CO production can be noticed. In order to quantify the
519 variations in CO produced from different concentrations of hydrogen, figure 16 shows the
520 distribution of CO mole fraction at the exit of fire holes.

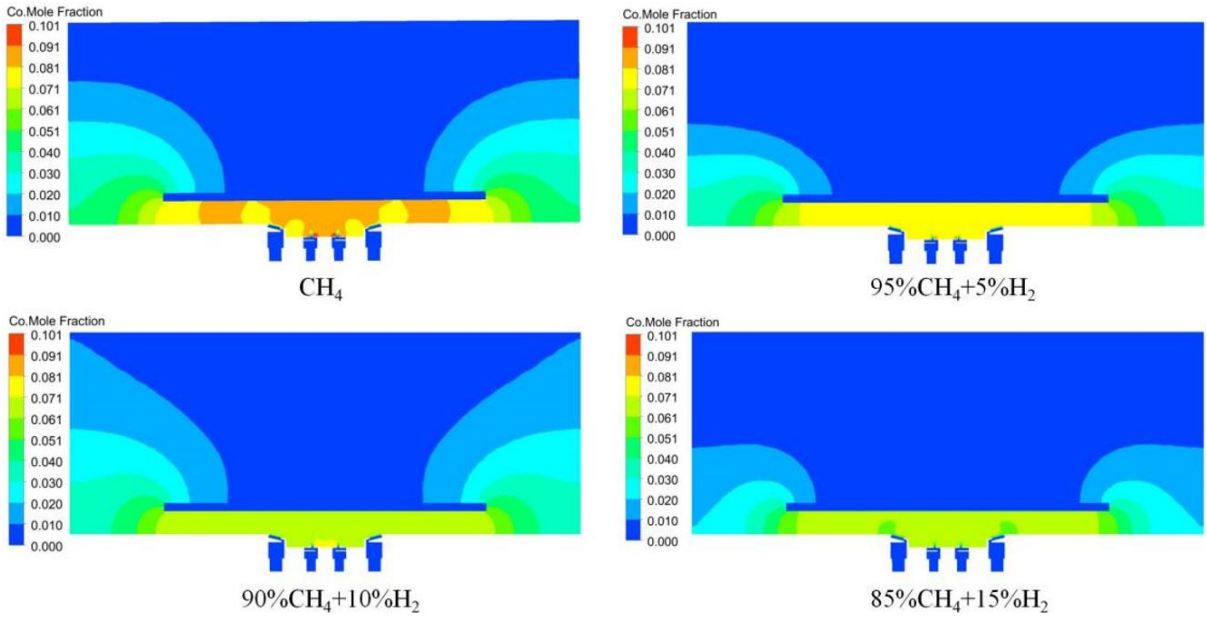

Figure 15. CO mole fraction variations for different volumetric concentrations of hydrogen

It can be seen in figure 16 that the mole fraction of CO remains almost constant at the exit of fire holes however, as the concentration of hydrogen increases, a significant decrease in CO production is observed. For pure methane combustion, the mole fraction of CO is ~ 0.083, which decreases to 0.074, 0.069 and 0.062 as hydrogen concentration increases to 5 %, 10 % and 15 % respectively. Thus, the decrease in CO mole fraction is 11 % (5 % H_2), 17 % (10 % H_2) and 25 % (15 % H_2).

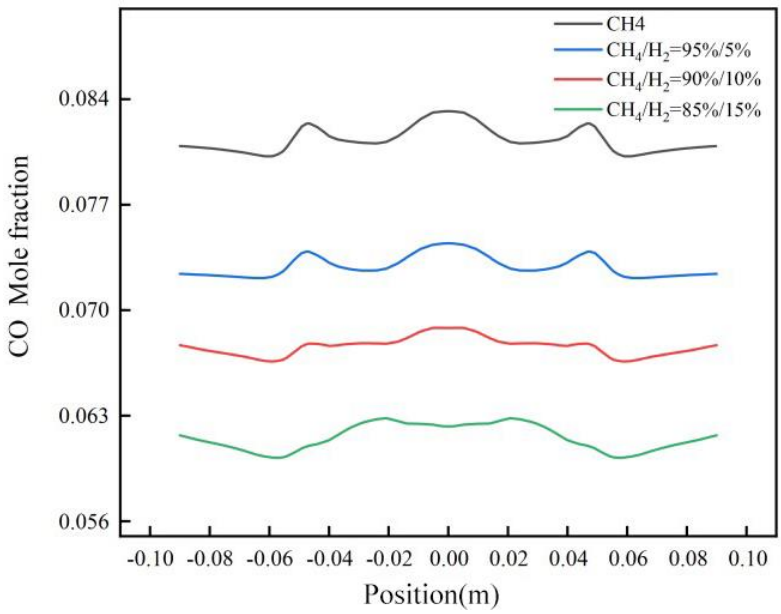

529

530 Figure 16. CO mole fraction distribution at the exit of fire holes for different concentrations

531 of hydrogen

532 The decrease in CO production from hydrogen doped methane is related to the products

533 of combustion reactions of methane and hydrogen. Generally speaking, the reaction path of

534 methane is $CH_4 \rightarrow CH_3 \rightarrow CH_2O \rightarrow HCO \rightarrow CO \rightarrow CO_2$, while the reaction path of hydrogen is

535 $H_2 \rightarrow HO_2/H \rightarrow OH \rightarrow H_2O$. Hydrogen reacts earlier and more violently than methane, which

536 improves the temperature of methane reaction. Since the minimum ignition energy of hydrogen

537 is 6% of that of natural gas, hydrogen is easy to ignite and starts the chemical reaction before

538 natural gas. After being ignited, hydrogen provides energy for the ignition of natural gas, so

539 the ignition temperature (initial reaction temperature) of the mixture composed of natural gas

540 and hydrogen increases. Therefore, adding hydrogen to methane can effectively reduce the

541 production of CO. The average concentrations of CO within the flow domain, resulting from

542 the combustion of hybrid methane-hydrogen mixture, is shown in figure 17. It can be seen that

543 as the concentration of hydrogen increases, the average concentration of CO in the flow domain

decreases. This decrease in CO mole fraction has been observed to be almost linear, which indicates that methane doped with 15 % of hydrogen (by volume) is the optimum combination for combustion in domestic swirl gas stoves.

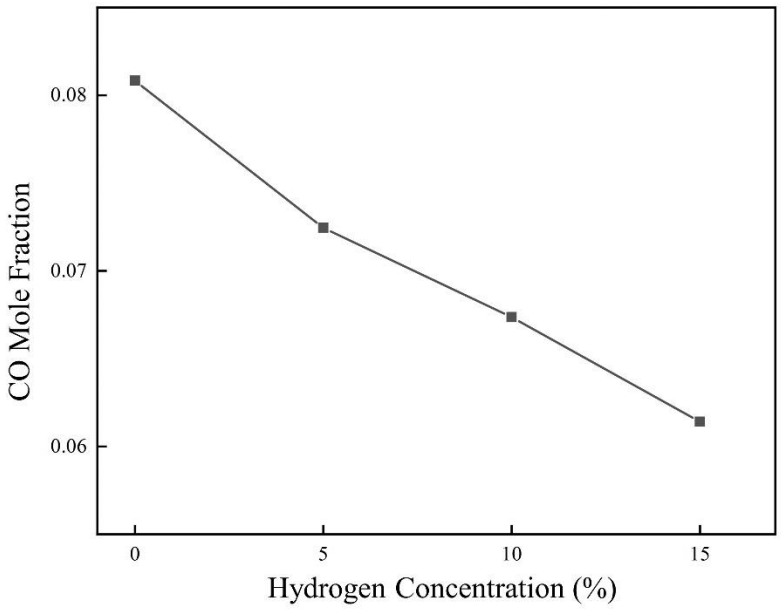

Figure 17. Variations in average CO mole fraction within the flow domain for different hydrogen concentrations

4.3 Experimental Validation of Hybrid Methane-Hydrogen Mixture Combustion

In order to validate the accuracy of the numerical simulations, combustion experiments have been conducted using hybrid 85 % Methane and 15 % Hydrogen mixture. The temperature distribution and carbon monoxide emissions have been measured and compared against the numerical results in figures 18 and 19. It has been found that the maximum temperature difference between the two data sets is < 5 %, while the maximum difference in CO mole fraction is < 3 %. Thus, it is evident that the numerically predicted results for the combustion of hybrid methane-hydrogen mixture are reasonably accurate.

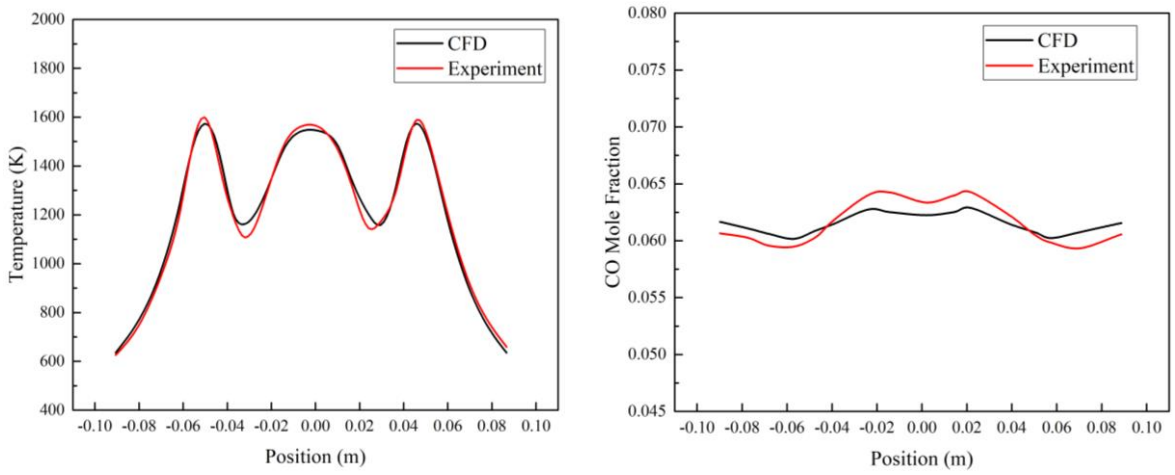

(a) (b)

Figure 18. Variations in (a) Temperature and (b) CO mole fraction for 15 % hydrogen concentration

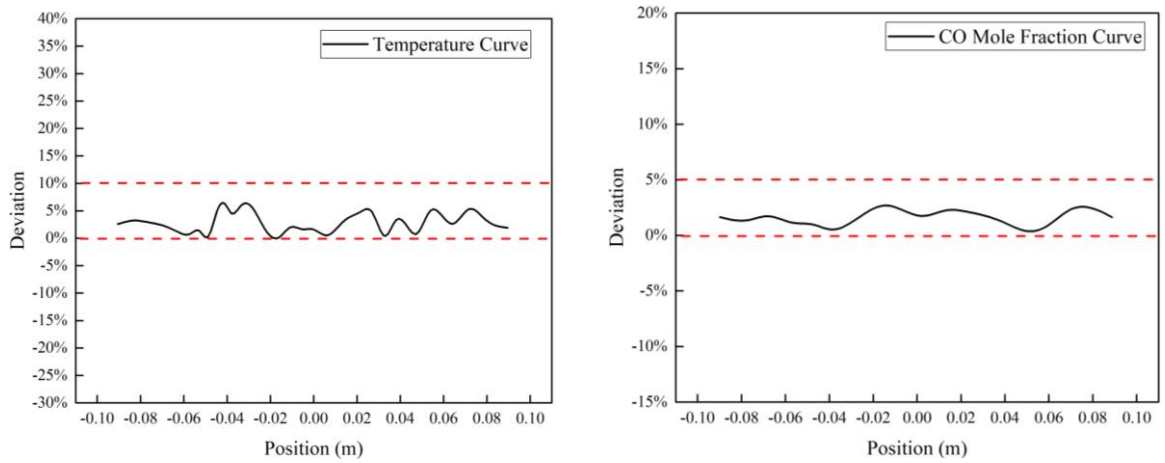

(a) (b)

Figure 19. Deviation between experimental and numerical (a) temperature and (b) CO mole fraction measurements

5.0 Conclusions

A simplified mechanism for the combustion of hybrid methane-hydrogen mixture has been developed based on the detailed model (GRI-Mech 3.0) using sensitivity analysis, direct relation graph and direct relation graph error propagation. The novel simplified mechanism has

been implemented with a conventional numerical solver (CFD) to investigate the combustion characteristics of hybrid methane-hydrogen gas mixture in a domestic swirl gas stove, and the results for temperature and CO mole fraction have been validated against hot-state test data. The main conclusions that can be drawn based on the results obtained are:

1. The simplified mechanism reduces the number of chemical reactions by 82 % compared to the conventional detailed mechanism, thus significantly reducing computational power requirements, while maintaining an accuracy of > 99 %.

2. For methane only combustion, the maximum difference between the numerical results and the experimental data is < 15 %, demonstrating the usefulness of the simplified mechanism.

3. For the combustion of hybrid methane-hydrogen mixture, the maximum difference between numerical and experimental data sets is < 5 %, while the maximum difference in CO mole fraction is < 3 %.

4. When methane is mixed with 15 % hydrogen by volumetric concentration, CO emission reduces by 25 %, while the combustion zone's average temperature reduces by 6.7 %.

5. For 15 % Hydrogen doped natural gas, the difference between numerically predicted and experimentally recorded temperature and CO mole fraction is < 5 % and < 3 % respectively, clearly demonstrating the accuracy of the simplified mechanism developed.

In this study, Hydrogen concentration of upto 15 % has been investigated. The influence of other mixing ratios of hydrogen (including mass ratio) on mixed fuel combustion has not been investigated. These investigations will become part of our follow-up research work.

Funding: This research did not receive any specific grant from funding agencies in the public, commercial, or not-for-profit sectors.

References

[1] Paris Agreement (2015) United Nations Framework Convention on Climate Change, T.I.A.S. 16-1104.

[2] British Petroleum report (2021) Statistical Review of World Energy, 70th edition. 2021.

[3] Zhang, S.H. Peng, X. and Yan, L.F. (2012) Smoke pollutants of domestic natural gas stoves under different flame combustion conditions; Chemical Progress, 234-238.

[4] Haeseldonckx, D. and D'haeseleer, W. (2007) The use of the natural-gas pipeline infrastructure for hydrogen transport in a changing market structure; International Journal of Hydrogen Energy (32) 1381-1386.

[5] Hu E, Huang Z, (2009) He J, et al. Experimental and numerical study on laminar burning characteristics of premixed methane–hydrogen–air flames, International Journal of Hydrogen Energy 34(11) 4876-4888.

[6] Donohoe N, Heufer A, Metcalfe W K, et al. (2014) Ignition delay times, laminar flame speeds, and mechanism validation for natural gas/hydrogen blends at elevated pressures, Combustion and Flame 161(6) 1432-1443.

[7] Ahmed A M, Desgroux P, Gasnot L, et al. (2016) Experimental and Numerical Study of rich methane/hydrogen/air Laminar Premixed Flames at Atmospheric Pressure: Influence of Hydrogen Addition on Soot Precursors, International Journal of Hydrogen Energy 41(16) 6929-6942.

610 [8] Ying Y, Liu D. (2015) Detailed influences of chemical effects of hydrogen as fuel additive
611 on methane flame, International Journal of Hydrogen Energy 40(9) 3777-3788.
612 [9] Luo, Z.X. Xu, H.C. and Yuan, M. (2019) Test and evaluation of the safety and emission
613 performance of the combustion of natural gas mixed with hydrogen on domestic gas appliances;
614 Oil and Gas Chemical Industry (48) 50-56.
615 [10] Zhao, Y. Vincent, M. and Samuelsen, S. (2019) Influence of hydrogen addition to pipeline
616 natural gas on the combustion performance of a cooktop burner; International Journal of
617 Hydrogen Energy (44) 12239-12253.
618 [11] Jiang, S.J. Liu, and Z.J. Zhang, C. (2009) Numerical Simulation Research on Swirl Gas
619 Stove; Thermal Science and Technology (8) 337-342.
620 [12] Chen, L. Feng, L. and Peng, W. (2020) Numerical simulation of high-power domestic gas
621 stove; Shanghai Gas (1) 4.
622 [13] Pashchenko, D. (2020) Hydrogen-rich fuel combustion in a swirling flame: CFD-
623 modeling with experimental verification; International Journal of Hydrogen Energy (45)
624 19996-20003.
625 [14] Sun, M. Huang, X. Hu, Y. (2022) Effects on the performance of domestic gas appliances
626 operated on natural gas mixed with hydrogen; Energy (244) 122557.
627 [15] Jones, D.R. Al-Masry, W.A. Dunnill, C. (2018) Hydrogen-enriched natural gas as a
628 domestic fuel: an analysis based on flash-back and blow-off limits for domestic natural gas
629 appliances within the UK; Sustainable Energy & Fuels (2) 710-723.
630 [16] Zhao, Y. McDonell, V. Samuelsen, S. (2019) Experimental assessment of the combustion
631 performance of an oven burner operated on pipeline natural gas mixed with hydrogen;

International Journal of Hydrogen Energy (44) 26049-26062.

[17] Gimeno-Escobedo, E. Cubero, A. Ochoa, J.S. (2019) A reduced mechanism for the prediction of methane-hydrogen flames in cooktop burners; International Journal of Hydrogen Energy (44) 27123-27140.

[18]Hou, J.L. Jin, P. and Cai, G.B. (2012) Simplified mechanism of oxygen/methane combustion reaction based on sensitivity analysis; Aerodynamics Journal (27) 1549-1554.

[19] Jiang, B. Ji, Q. and Zhao, C.P. (2016) Simplification mechanism of methane/air combustion and its application; Journal of Henan University of Science and Technology (37) 24-28.

[20] Wang, L.Y. Wang, Z.F. and Chen, W.H. (2020) Simplified detailed chemical reaction mechanism of high-temperature combustion of phenolic resin pyrolysis products; Journal of Nanjing University of Aeronautics and Astronautics (52) 131-141.

[21] Ruan, D. Qi, Y.Y. and Li, H.D. (2016) Numerical simulation study of NO reduction by CO at high temperature without catalyst; Silicate Journal (35) 1674-1681.

[22] Lu, T.F. and Law, C.K. (2005) A directed relation graph method for mechanism reduction; Proceedings of the Combustion Institute (30) 1333-1341.

[23] Fany, Y.M. Wany, Q.D. Wany, F. and Li, X.Y. (2012) Reduction of the Detailed Kinetic Mechanism for High-Temperature Combustion of n-Dodecane; Acta Physico-Chimica Sinica (28) 2536-2542(7).

[24] Lu, T. and Law, C.K. (2006) Linear time reduction of large kinetic mechanisms with directed relation graph: n-Heptane and iso-octane; Combustion and Flame (144) 24-36.

[25] Poon, H. Ng, H. Gan, S. and Pang, K. (2013) Evaluation and Development of Chemical

654 Kinetic Mechanism Reduction Scheme for Biodiesel and Diesel Fuel Surrogates; SAE
655 International Journal of Fuels and Lubricants (6) 729-744.
656 [26] Monnier, F. Ribert, G. (2022) Simulation of high-pressure methane-oxygen combustion
657 with a new reduced chemical mechanism; Combustion and Flame (235) 111735.
658 [27] Niemeyer, K.E. Sung, C. Raju, M.P. (2010) Skeletal mechanism generation for surrogate
659 fuels using directed relation graph with error propagation and sensitivity analysis; Combustion
660 and flame (157) 1760-1770.
661 [28] Tang, A. Huang, Q. Li, Y. (2022) Development and verification of simplified
662 methane/dimethyl ether mechanism for micro-combustion; Fuel Processing Technology (226)
663 107071.
664 [29] Zheng, X.L. Lu, T.F. Law, C.K. (2007) Experimental counterflow ignition temperatures
665 and reaction mechanisms of 1, 3-butadiene; Proceedings of the Combustion Institute (31) 367-
666 375.
667 [30] Hu, F. Li, P. Guo, J. (2018) Evaluation, development, and validation of a new reduced
668 mechanism for methane oxy-fuel combustion; International Journal of Greenhouse Gas Control
669 (78) 327-340.
670 [31] Li, R. Konnov, A.A. He, G. (2019) Chemical mechanism development and reduction for
671 combustion of NH3/H2/CH4 mixtures; Fuel (257) 116059.
672 [32] CHEMKIN 10112 (2011) Reaction Design: San Diego, USA.
673 [33] Glarborg, P. Kee, R.J. Grcar, J.F. (1986) PSR: A FORTRAN program for modeling well
674 stirred reactors; Sandia National Laboratories Livermore, CA, USA.
675 [34] Luo, D.D. Zhen, H.S. Leung, C.W. (2010) Premixed flame impingement heat transfer with

676 induced swirl; International Journal of Heat and Mass Transfer (53) 4333-4336.
677 [35] ANSYS, Inc. (2022) ANSYS Fluent User's Guide, Release 22R1.
678 [36] Singh, D. Aliyu, A.M. Charlton, M. Mishra, R. Asim, T. and Oliveira, A.C. (2020) Local
679 multiphase flow characteristics of a severe-service control valve; Journal of Petroleum Science
680 and Engineering (195) 107557.
681 [37] Asim, T. Mishra, R. Kaysthagir, S. and Aboufares, G. (2015) Performance Comparison of
682 a Vertical Axis Wind Turbine using Commercial and Open-Source Computational Fluid
683 Dynamics based Codes; In the proceedings of the International Conference on Jets, Wakes and
684 Separated Flows, Stockholm, Sweden.
685 [38] Hindasageri, V. Kuntikana, P. Vedula, R.P. and Prabhui, S.V. (2015) An experimental and
686 numerical investigation of heat transfer distribution of perforated plate burner flames
687 impinging on a flat plate; International Journal of Thermal Sciences (94) 156-169.
688 [39] Zheng, H.F. (2018) Analysis of Heat Loss of Gas Stove and Efficient Gas stove, Huazhong
689 University of Science & Technology, China.
690 [40] Jin, L. Zhou, J.S. and Wu, Y.M. (2011) Research on Gasification Performance of
691 Downdraft Biomass Gasifier; Thermal Power Engineering (26) 105-109.
692 [41] Galletti, C. Giovanni, C. and Leonardo, T. (2013) Numerical investigation of oxy-natural-
693 gas combustion in a semi-industrial furnace: Validation of CFD sub-models; Fuel (109) 445-
694 460.
695 [42] Su, Y. Chen, C. and Su, A. (2012) Simulation of high temperature air combustion with
696 modified eddy-break-up combustion model; Energy Procedia (14) 127-132.
697 [43] Yin, C. (2017) Prediction of air-fuel and oxy-fuel combustion through a generic gas

698 radiation property model; Applied Energy (189) 449-459.

699 [44] Wu, C. (2018) Feasibility study on Blending hydrogen into Natural gas Distribution

700 Networks; Chongqing University, China.

701 [45] Craig, M. and Asim, T. (2020) Numerical Investigations on the Propagation of Fire in a

702 Railway Carriage; Energies (13) 4999.

703

704 **Appendix**

705 Simplified reaction model

706

1	2O+M=O2+M	30	OH+CH4=CH3+H2O
2	O+H+M=OH+M	31	OH+CO=H+CO2
3	O+H2=H+OH	32	HO2+CH3=O2+CH4
4	O+HO2=OH+O2	33	HO2+CO=OH+CO2
5	O+CH2(S)=H2+CO	34	CH2+O2=>OH+H+CO
6	O+CH4=OH+CH3	35	CH2+H2=H+CH3
7	O+CO(+M)=CO2(+M)	36	CH2+CH4=2CH3
8	O2+CO=O+CO2	37	CH2(S)+N2=CH2+N2
9	H+O2+M=HO2+M	38	CH2(S)+O2=H+OH+CO
10	H+2O2=HO2+O2	39	CH2(S)+O2=CO+H2O
11	H+O2+H2O=HO2+H2O	40	CH2(S)+H2=CH3+H
12	H+O2+N2=HO2+N2	41	CH2(S)+H2O=CH2+H2O
13	H+O2=O+OH	42	CH2(S)+CH4=2CH3

14	2H+M=H2+M	43	CH2(S)+CO=CH2+CO
15	2H+H2=2H2	44	CH2(S)+CO2=CH2+CO2
16	2H+H2O=H2+H2O	45	N+NO=N2+O
17	2H+CO2=H2+CO2	46	N+O2=NO+O
18	H+OH+M=H2O+M	47	N+OH=NO+H
19	H+HO2=O+H2O	48	NNH=N2+H
20	H+HO2=O2+H2	49	NNH+M=N2+H+M
21	H+HO2=2OH	50	NNH+O2=HO2+N2
22	H+CH2(+M)=CH3(+M)	51	NNH+O=OH+N2
23	H+CH3(+M)=CH4(+M)	52	NNH+H=H2+N2
24	H+CH4=CH3+H2	53	NNH+OH=H2O+N2
25	OH+H2=H+H2O	54	NNH+CH3=CH4+N2
26	2OH=O+H2O	55	N+CO2=NO+CO
27	OH+HO2=O2+H2O	56	O+CH3=>H+H2+CO
28	OH+CH3=CH2+H2O	57	OH+HO2=O2+H2O
29	OH+CH3=CH2(S)+H2O	58	CH2+O2=>2H+CO2